ACS OMEGA

Article

http://pubs.acs.org/journal/acsodf

Toward Positive Electrode Materials with High-Energy Density: Electrochemical and Structural Studies on $LiCo_xMn_{2-x}O_4$ with $0 \leq x \leq 1$

Kazuhiko Mukai* and Takeshi Uyama

Toyota Central Research & Development Laboratories, Inc., 41-1 Yokomichi, Nagakute, Aichi 480-1192, Japan

Supporting Information

ABSTRACT: To obtain positive electrode materials with higher energy densities (*W*s), we performed systematic structural and electrochemical analyses for $LiCo_xMn_{2-x}O_4$ (LCMO) with $0 \leq x \leq 1$. X-ray diffraction measurements and Raman spectroscopy clarified that the samples with $x \leq 0.5$ are in the single-phase of a spinel structure with the $Fd\bar{3}m$ space group, whereas the samples with $x \geq 0.75$ are in a mixture of the spinel-phase and Li_2MnO_3 phase with the $C2/m$ space group. The *x*-dependence of the discharge capacity (Q_{dis}) indicated a broad maximum at $x = 0.5$, although the average operating voltage (E_{ave}) monotonically increased with *x*. Thus, the *W* value obtained by $Q_{dis} \times E_{ave}$ reached the maximum (=627 mW h·g^{-1}) at $x = 0.5$, which is greater than that for $Li[Ni_{1/2}Mn_{3/2}]O_4$. Furthermore, the change in the lattice volume (ΔV) during charge and discharge reactions approached 0%, that is, zero-strain, at $x = 1$. Because ΔV for $x = 0.5$ was smaller than that for $Li[Ni_{1/2}Mn_{3/2}]O_4$, the $x = 0.5$ sample is found to be an alternative positive electrode material for $Li[Ni_{1/2}Mn_{3/2}]O_4$ with a high *W*.

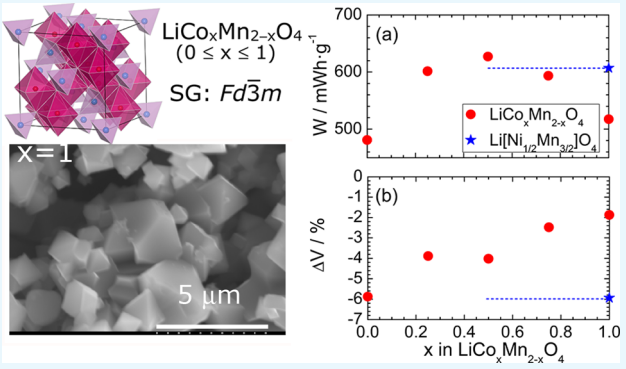

1. INTRODUCTION

The bottom line of batteries in baseball is the harmonizing of a pitcher and a catcher. In the same way, the balancing of the electrochemical performances between a positive electrode and a negative electrode is crucial for secondary batteries. As previously reviewed for lithium-ion batteries (LIBs),[1,2] the energy densities (*W*s) for positive electrode materials are significantly lower than those for negative electrode materials. This imbalanced situation still restricts the widespread applications of LIBs, such as in electric vehicles (EVs) and stationary energy storage systems (ESSs).[1] In other words, positive electrode materials with higher *W*s are urgently required to realize more practical EVs and ESSs.

The *W* value for a positive electrode material is determined as follows

$$W = \int Q_{recha}\, dQ \times E_{ave} \quad (1)$$

where Q_{recha} is the rechargeable capacity and E_{ave} is the average operation voltage. Therefore, a positive electrode material with a high Q_{recha} or a high E_{ave} or both provides a high *W*. Over the past decade, lithium−nickel−manganese spinel $Li[Ni_{1/2}Mn_{3/2}]O_4$ has attracted much attention because it offers ∼135 mA h·g^{-1} of Q_{recha} and 4.5 V versus Li^+/Li of E_{ave}, resulting in more than 600 mW h·g^{-1} of *W*.[3−6] Lithium−cobalt−manganese spinel $LiCo_xMn_{2-x}O_4$ (LCMO) with $0 \leq x \leq 1$ is also promising from the viewpoint of E_{ave};[7−13] namely, the redox reaction of $Co^{3+} \leftrightarrow Co^{4+}$ in LCMO is ∼0.3 V higher than that of $Ni^{2+} \leftrightarrow Ni^{4+}$ in $Li[Ni_{1/2}Mn_{3/2}]O_4$.[3,4,8,9,11]

Previous X-ray absorption near-edge structure (XANES)[8] analyses and magnetic measurements of electron paramagnetic resonance (EPR)[14,15] and susceptibility[16] indicated that Co ions in LCMO are in the trivalent state with a low-spin t_{2g}^6 ($S = 0$) configuration. The ideal electrochemical reaction of LCMO is thus represented as

$$LiCo_x^{3+}Mn_{1-x}^{3+}Mn^{4+}O_4 \rightarrow Li^+ + e^- + Co_x^{4+}Mn_{1-x}^{4+}Mn^{4+}O_4 \quad (2)$$

where the theoretical capacity (Q_{theo}) is calculated to be (148.23 − 3.21*x*) mA h·g^{-1}. The current Q_{recha} for $x = 1$ is, however, significantly lower than Q_{theo} and is usually[7−11] limited to ∼100 or 116 mA h·g^{-1} at the maximum.[13] This comes from the presence of Li_2MnO_3 impurities in $x = 1$, which are electrochemically inactive.[9] By contrast, the E_{ave} for LCMO almost linearly increases on increasing the amount of the $Co^{3+} \leftrightarrow Co^{4+}$ redox reaction. Because *W* is the product obtained by the multiplication of Q_{recha} and E_{ave}, as shown by eq 1, the opposite trend between Q_{recha} and E_{ave} in LCMO is expected to indicate a maximum *W* value at a certain *x* composition. Despite the intensive studies on LCMO thus far,[7−16] a

Received: July 7, 2017
Accepted: August 15, 2017
Published: August 29, 2017

DOI: 10.1021/acsomega.7b00948
ACS Omega 2017, 2, 5142−5149

systematic study to explore the optimum x composition for the highest W has not been undertaken.

In this contribution, we report the results of Q_{recha}, E_{ave}, and W as a function of x in LCMO and compare them with $Li[Ni_{1/2}Mn_{3/2}]O_4$. Structural analyses using synchrotron radiation X-ray diffraction (XRD) measurements and Raman spectroscopy were also performed to clarify the relation between the electrochemical properties and crystal structures of LCMO. Consequently, we revealed that the x = 0.5 composition provides the maximum W value of 627 mW h·g^{-1}, with a change in the lattice volume of ∼4%. These performances were found to be superior to those of $Li[Ni_{1/2}Mn_{3/2}]O_4$.

2. RESULTS AND DISCUSSION

2.1. Particle Morphology. For positive electrode materials with high E_{ave} values, the particle size and morphology significantly affect their electrochemical properties,[17] probably due to the decomposition of electrolytes. To clarify changes in the particle size and morphology with x, Figure 1 shows the

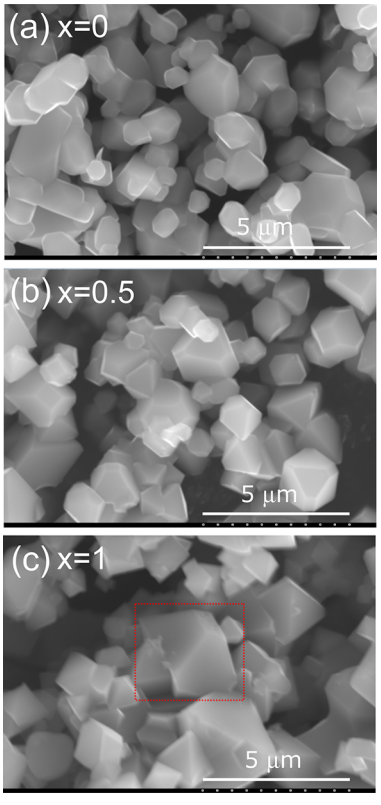

Figure 1. SEM images on the 5 μm scale for the $LiCo_xMn_{2-x}O_4$ samples with (a) x = 0, (b) x = 0.5, and (c) x = 1. One of the particles in the x = 1 sample (surrounded by the red dotted line) shows a truncated octahedron with a facet growth velocity ratio (α) of 2.25 < α < 2.5.

scanning electron microscopy (SEM) images for the LCMO samples with (a) x = 0, (b) x = 0.5, and (c) x = 1. The x = 0 sample indicates a nonuniform particle shape with an average particle size (d_{ave}) of 2 μm. For the x = 0.5 and 1 samples, some particles show a truncated octahedral shape, although their d_{ave} values are similar to that of the x = 0 sample. As seen in Figure S1, particles for the x = 0.25 and 0.5 samples also show a truncated octahedral shape with d_{ave} of ∼2 μm. Thus, the substitution of Co ions for Mn ions mainly influences the particle morphology for LCMO.

The $Li[Ni_{1/2}Mn_{3/2}]O_4$ particles prepared by the two-step solid-state reaction technique exhibit an octahedral shape with smooth {111} facets, not a truncated octahedral shape.[17] The difference between the octahedral and truncated octahedral shapes originates from the proportion of the {001} facets to {111} facets. One simple method to quantitatively describe such a difference is given by the Wulff construction[18]

$$\alpha = \sqrt{3}\frac{V_{001}}{V_{111}} \quad (3)$$

where α is the facet growth velocity ratio and V_{001} and V_{111} are the growth velocities of the {001} and {111} facets, respectively. When α = 1, the particle indicates only the {001} facets, that is, cubic, whereas when α = 3, the particle indicates only the {111} facets, that is, regular octahedron.[18] As seen from the x = 1 particle surrounded by a red dotted line in Figure 1c, the surface area of one {001} facet is estimated to be 1.1 μm^2, whereas that of one {111} facet is estimated to be 3.9 μm^2. Thus, the ratio of the {001} facets to {111} facets is estimated to be ∼0.2, resulting in 2.25 < α < 2.5.

2.2. Electrochemistry. Figure 2 shows the charge and discharge curves of the LCMO/Li cells with (a) x = 0, (b) x =

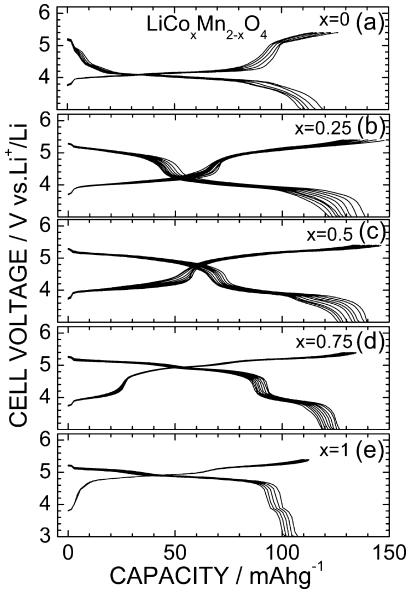

Figure 2. Charge and discharge curves of the $LiCo_xMn_{2-x}O_4$/Li cells with (a) x = 0, (b) x = 0.25, (c) x = 0.5, (d) x = 0.75, and (e) x = 1. The cells were operated at a current of 0.6 mA (0.3 mA·cm^{-2}) in the voltage range between 3.0 and 5.4 V at 25 °C.

0.25, (c) x = 0.5, (d) x = 0.75, and (e) x = 1. For the x = 0 sample, the cell voltage rapidly increases to ∼4.0 V, then maintains an almost constant voltage at around 4.2 V up to a charge capacity (Q_{cha}) of ∼80 mA h·g^{-1}, and finally indicates another voltage plateau at around 5.2 V. The voltage plateau above 5.0 V is also reported for the charge curves for $Li[Li_xMn_{2-x}]O_4$ with $0 \le x \le 1/3$.[19,20] The Q_{cha} and discharge capacity (Q_{dis}) at the initial cycle are 126 and 119 mA h·g^{-1}, respectively. For the x = 0.25 and 0.5 samples, the Q_{cha} values below ∼4.0 V decrease compared with that for x = 0; and in turn, the Q_{cha} values above ∼5.0 V increase with x. The Q_{cha} and Q_{dis} values at the initial cycle are not different between the

DOI: 10.1021/acsomega.7b00948
ACS Omega 2017, 2, 5142−5149

x = 0.25 and 0.5 samples; that is, the Q_{cha} and Q_{dis} values are 147 and 138 mA h·g^{-1}, respectively, for x = 0.25, and the Q_{cha} and Q_{dis} values are 146 and 140 mA h·g^{-1}, respectively, for x = 0.5. However, as clearly seen from the intersecting voltages between the charge and discharge curves, the E_{ave} value for x = 0.5 is expected to be greater than that for x = 0.25.

For the x = 0.75 sample, the Q_{cha} value at around 4.0 V is decreased to ∼25 mA h·g^{-1}; however, the whole Q_{cha} (=134 mA h·g^{-1}) and Q_{dis} (=127 mA h·g^{-1}) values at the initial cycle are slightly decreased compared with those for x = 0.25 and 0.5. For the x = 1 sample, the Q_{cha} and Q_{dis} values at the initial cycle are further decreased to 112 and 108 mA h·g^{-1}, respectively, in exchange for the almost disappearance of the Q_{cha} value at around 4.0 V. Such Q_{cha} and Q_{dis} values are similar to the reported values for x = 1.[7−13] According to the previous XANES analyses[8] and EPR measurements,[14,15] the electrochemical reaction at around 4.0 V is attributed to the redox reaction of $Mn^{3+} \leftrightarrow Mn^{4+}$, whereas that at around 5.0 V is attributed to the redox reaction of $Co^{3+} \leftrightarrow Co^{4+}$. The small amount of Q_{dis} at around 4.0 V in x = 1 indicates that the Mn^{3+} ions still exist in the sample, although its ideal chemical formula is described as $Li[Co^{3+}Mn^{4+}]O_4$. Figure S2 shows the charge and discharge curves for the x = 1 sample prepared at 1000 and 1100 °C. As the maximum heating temperature increases, the Q_{dis} value decreases; for example, Q_{dis} = 72 mA h·g^{-1} for 1100 °C. This is because the amount of the Li_2MnO_3 impurity increases, as later shown in Figures 4c and 6c.

Figure 3 shows the x-dependence of (a) Q_{dis} at the initial cycle, (b) E_{ave} of the initial discharge curve, and (c) W obtained by $Q_{dis} \times E_{ave}$. Results of $Li[Ni_{1/2}Mn_{3/2}]O_4$ with the $P4_332$ space group[5] are also shown for comparison. The x-dependence of Q_{dis} indicates a broad maximum at around x = 0.5, whereas E_{ave} almost monotonically increases from 4.166 V at x = 0 to 4.996 V at x = 1. The observed Q_{dis} is lower than the calculated Q_{theo} over the whole x range. Consequently, W gradually increases from 480 mW h·g^{-1} at x = 0, then reaches the maximum (=627 mW h·g^{-1}) at x = 0.5, and finally decreases to 516 mW h·g^{-1} at x = 1. The maximum W value for x = 0.5 is slightly greater than that for $Li[Ni_{1/2}Mn_{3/2}]O_4$ (=607 mW h·g^{-1}), and as far as we are concerned, the x-dependence of W in LCMO has been clarified for the first time because previous studies on LCMO were focused on the Q_{dis} values.[7−16]

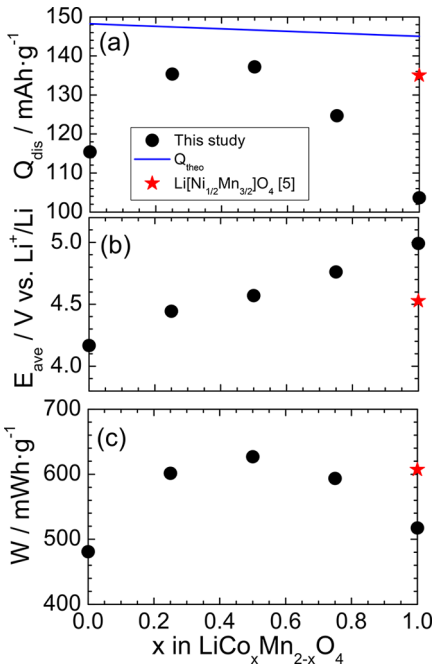

Figure 3. Results of the electrochemical measurements for the $LiCo_xMn_{2-x}O_4$ samples with $0 \le x \le 1$: (a) discharge capacity at the initial cycle (Q_{dis}), (b) average voltage (E_{ave}) of the initial discharge curve, and (c) energy density (W) obtained by $Q_{dis} \times E_{ave}$. The solid line indicates the Q_{theo} for LCMO calculated by (148.23 − 3.21x) mA h·g^{-1}. The results for $Li[Ni_{1/2}Mn_{3/2}]O_4$ with the $P4_332$ space group are taken from ref 5.

2.3. Crystal Structure. In this section, we examined the crystal structures before and after the charge reaction to understand the electrochemical reaction scheme of LCMO. Figure 4 shows the results for the Rietveld analyses for the pristine (a) x = 0, (b) x = 0.5, and (c) x = 1 samples. The crystal structure for x = 0 is assigned as a spinel structure with the $Fd\bar{3}m$ space group, in which Li^+ and Mn^{3+}/Mn^{4+} ions occupy tetrahedral 8a and octahedral 16d sites, respectively. Structural parameters, such as the cubic lattice parameter a_c [=8.2225(1) Å] and oxygen positional parameter u [=0.264(1)], are consistent with the previous results for $LiMn_2O_4$ (Table 1).[19−21]

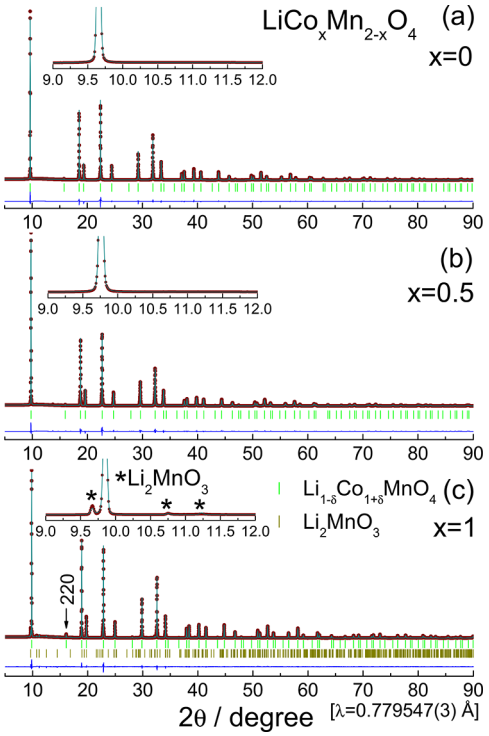

Figure 4. Results of the Rietveld analyses for the pristine $LiCo_xMn_{2-x}O_4$ samples with (a) x = 0, (b) x = 0.5, and (c) x = 1. Enlarged XRD patterns are also shown in the insets to clarify the presence of the Li_2MnO_3 phase (indicated by *). The 220 diffraction in x = 1 indicates the presence of Co ions at the tetrahedral 8a site.

Before describing the result for x = 0.5, we wish to mention the result for x = 1. The majority of the x = 1 sample is in the $Fd\bar{3}m$ space group, as in the case for x = 0. However, as seen in the inset of Figure 4c, the diffraction lines indicated by * are clearly observed in the vicinity of the diffraction line around 2θ = 10° (the 111 diffraction line of the spinel structure). These diffraction lines originate from the Li_2MnO_3 phase with the monoclinic structure, whose weight fraction is determined to be

DOI: 10.1021/acsomega.7b00948
ACS Omega 2017, 2, 5142−5149

Table 1. Structural Parameters for the Pristine $LiCo_xMn_{2-x}O_4$ Samples with x = 0, 0.25, 0.5, 0.75, and 1 Determined by the Rietveld Analyses

x in $LiCo_xMn_{2-x}O_4$	atom	Wyckoff position	occupancy	atomic coordination			B_{iso} (Å^2)
				x	y	z	
		SG: $Fd\bar{3}m$, a_c = 8.2226(1) Å, R_{wp} = 5.78%, and S = 0.513					
x = 0	Li	8a	1.00	0.125	0.125	0.125	0.86(1)
	Mn	16d	1.00	0.5	0.5	0.5	0.61(1)
	O	32e	1.00	0.264(1)	0.264(1)	0.264(1)	0.87(1)
		SG: $Fd\bar{3}m$, a_c = 8.1595(1) Å, R_{wp} = 5.21%, and S = 0.439					
x = 0.25	Li	8a	1.00	0.125	0.125	0.125	0.67(1)
	Co2	16d	0.125	0.5	0.5	0.5	0.45(1)
	Mn	16d	0.875	0.5	0.5	0.5	0.45(1)
	O	32e	1.00	0.264(1)	0.264(1)	0.264(1)	0.52(1)
		SG: $Fd\bar{3}m$, a_c = 8.1300(1) Å, R_{wp} = 7.39%, and S = 0.647					
x = 0.5	Li	8a	1.00	0.125	0.125	0.125	1.2(1)
	Co	16d	0.25	0.5	0.5	0.5	0.37(1)
	Mn	16d	0.75	0.5	0.5	0.5	0.37(1)
	O	32e	1.00	0.264(1)	0.264(1)	0.264(1)	0.50(1)
		SG: $Fd\bar{3}m$, a_c = 8.0791(1) Å, R_{wp} = 6.99%, and S = 0.582					
x = 0.75	Li	8a	0.970(1)	0.125	0.125	0.125	0.76(1)
	Co1	8a	0.030(1)	0.125	0.125	0.125	0.76(1)
	Co2	16d	0.371(1)	0.5	0.5	0.5	0.26(1)
	Mn	16d	0.629(1)	0.5	0.5	0.5	0.26(1)
	O	32e	1.00	0.264(1)	0.264(1)	0.264(1)	0.37(1)
		SG: $Fd\bar{3}m$, a_c = 8.0589(1) Å, R_{wp} = 6.42%, and S = 0.532.					
x = 1	Li	8a	0.887(1)	0.125	0.125	0.125	0.43(1)
	Co1	8a	0.113(1)	0.125	0.125	0.125	0.43(1)
	Co2	16d	0.5(1)	0.5	0.5	0.5	0.22(1)
	Mn	16d	0.5(1)	0.5	0.5	0.5	0.22(1)
	O	32e	1.00	0.264(1)	0.264(1)	0.264(1)	0.52(1)

6.23%. Coexistence of the Li_2MnO_3 phase is also reported in previous structural analyses on x = 1.[9] Moreover, the intensity of the 220 diffraction line at around 2θ = 17° is slightly larger than that for x = 0 [compare Figure 4a,c], indicating that a small amount of metal (Co) ions exists in the tetrahedral 8a site. As a result, the crystal structure for the x = 1 sample is assigned as a mixture of the spinel phase with the $Fd\bar{3}m$ space group and the Li_2MnO_3 impurity with the $C2/m$ space group. Because the amount of Co ions at the 8a site is determined to be 0.113(1), the actual formula for x = 1 can be represented as $Li_{0.887}Co_{0.113}[CoMn]O_4$. Note that the mixture of 93.77 wt % $Li_{0.887}Co_{0.113}[CoMn]O_4$ and 6.23 wt % Li_2MnO_3 is consistent with the Li/Co/Mn (=1/1/1) composition of the starting material: mol % of $Li_{0.887}Co_{0.113}[CoMn]O_4$ and Li_2MnO_3 are calculated to be 89.3 and 10.7, respectively, providing the composition of Li/Co/Mn = 1.01/0.99/1.00.

The Li_2MnO_3 impurity is not observed in the x = 0.5 sample [see Figure 4b]. The crystal structure for x = 0.5 is thus assigned as the single-phase of the spinel structure with the $Fd\bar{3}m$ space group. Figure S3 shows the results for the Rietveld analyses for the pristine (a) x = 0.25 and (b) x = 0.75 samples. The situation for x = 0.25 is similar to that for x = 0.5; the sample crystallized into a single-phase of the spinel structure. By contrast, the Li_2MnO_3 impurity was observed in the XRD pattern for the x = 0.75 sample [see diffraction lines indicated by * in Figure S3b]. The weight fraction of the Li_2MnO_3 phase in x = 0.75 is determined to be 1.67%, and the actual formula for x = 0.75 can be represented as $Li_{0.970}Co_{0.030}[CoMn]O_4$. As seen from Figure S4, the amount of the Li_2MnO_3 phase in LCMO rapidly increases at $x \geq 0.75$.

We next examined the distributions of the Li_2MnO_3 phase in the x = 1 sample by Raman spectroscopy. Figure S5 shows the Raman spectra for the LCMO samples with $0 \leq x \leq 1$. According to a factor group analysis,[22] five Raman active modes of $A_{1g} + E_g + 3F_{2g}$ are predicted for the spinel structure with the $Fd\bar{3}m$ space group. The Raman spectrum for x = 0 shows a major Raman band at around 623 cm^{-1} and three minor Raman bands at 572, 477, and 365 cm^{-1}. The major Raman band is assigned as the A_{1g} mode, which corresponds to a symmetric vibration between Mn^{3+}/Mn^{4+} and O^{2-} ions.[16,23] The major Raman band at around 623 cm^{-1} splits into two or three Raman bands with x, probably due to the change in the proportion of Mn^{3+}/Mn^{4+} ions.[16] As seen in Figure 5a, the x = 1 sample indicates three major Raman bands at around 652, 575, and 538 cm^{-1} and three minor Raman bands at around 475, 382, and 179 cm^{-1}. Although these Raman bands are still unassigned, the Raman spectrum for x = 1 significantly differs from that for the single-phase of Li_2MnO_3 [Figure 5b]. This enables the $LiCoMnO_4$ sample to be distinguished into $Li_{0.887}Co_{0.113}[CoMn]O_4$ and Li_2MnO_3 phases. As provided in Figure 5c, the Li_2MnO_3 phase segregates from the $Li_{0.887}Co_{0.113}[CoMn]O_4$ phase, not coexisting in the $Li_{0.887}Co_{0.113}[CoMn]O_4$ phase.

Figure 6 shows the results of the Rietveld analyses for the fully charged LCMO samples with (a) x = 0, (b) x = 0.5, and (c) x =1. Figure S6 shows the results of the fully charged LCMO samples with (a) x = 0.25 and (b) x = 0.75. Here "fully" means the lithium cells were charged up to 5.4 V before the XRD measurements. The y values were calculated to be y = 0.15 for x = 0, $y \approx 0$ for x = 0.25, $y \approx 0$ for x = 0.5, y = 0.08 for x = 0.75, and y = 0.228 for x = 1, by ignoring the capacities

DOI: 10.1021/acsomega.7b00948
ACS Omega 2017, 2, 5142−5149

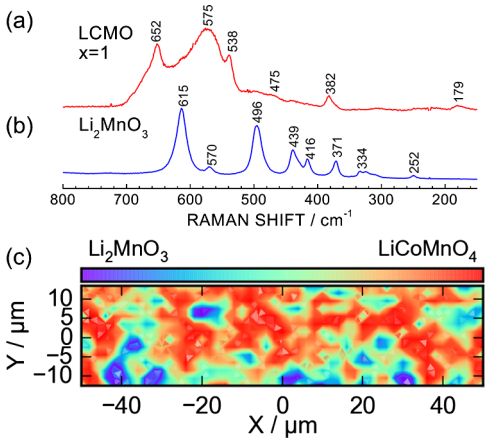

Figure 5. Raman spectra for the (a) $LiCo_xMn_{2-x}O_4$ sample with $x = 1$ and (b) Li_2MnO_3. (c) Two-dimensional Raman mapping for the $x = 1$ sample in the region of width 100 μm and height 25 μm. The regions of $Li_{1-\delta}Co_{1+\delta}MnO_4$ and Li_2MnO_3 phases are shown by red and blue, respectively.

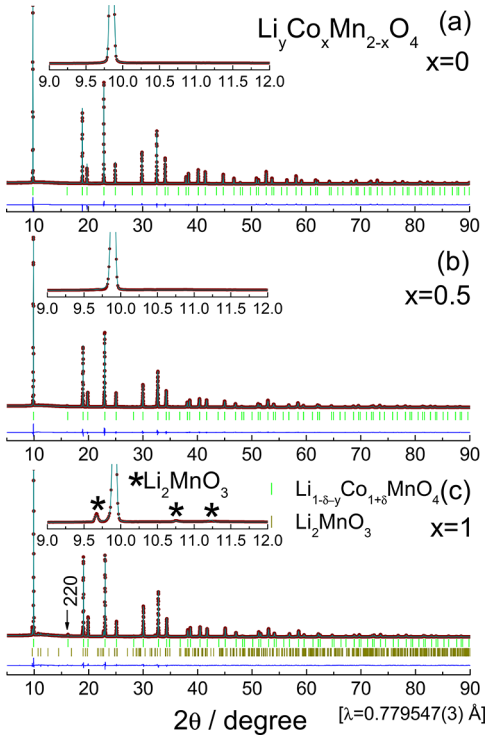

Figure 6. Results of the Rietveld analyses for the fully charged $Li_yCo_xMn_{2-x}O_4$ samples with (a) $x = 0$, (b) $x = 0.5$, and (c) $x = 1$. All samples were prepared using the electrochemical reaction charging up to 5.4 V. Enlarged XRD patterns are also shown in the insets to clarify the presence of the Li_2MnO_3 phase (indicated by *). The 220 diffraction in $x = 1$ indicates the presence of Co ions at the tetrahedral 8a site.

consumed for electrolyte decompositions. As seen from Figures 6 and S6, all LCMO samples maintain a spinel structure with the $Fd\bar{3}m$ space group, as in the cases for the initial (pristine) state. Structural parameters, such as a_c and u, are summarized in Table 2.

2.4. Δa_c and ΔV for LCMO. Figure 7a shows the a_c values before and after the fully charged reaction as a function of x in $LiCo_xMn_{2-x}O_4$. The a_c value before the charge reaction (pristine sample) monotonically decreases from 8.2225(1) Å at $x = 0$ to 8.0589(1) Å at $x = 1$. This linear decrease in a_c agrees with the change in the ionic radius (r) from Mn^{3+} ions with CN = 6 ($r_{Mn^{3+}} = 0.58$ Å) to Co^{3+} ions ($r_{Co^{3+}} = 0.55$ Å) with CN = 6, where CN is the coordination number.[24] The a_c value after the fully charged reaction also indicates a linear decrease in a_c with x, however, its slope (a_c/x) is much smaller than that for the LCMO samples before the charge reaction. That is, the a_c value slightly decreases from 8.0581(1) Å at $x = 0$ to 8.0083(1) Å at $x = 1$.

Using these a_c values for LCMO, the change in a_c (Δa_c) and the change in the lattice volume (ΔV) are determined. As seen in Figure 7b, both Δa_c and ΔV values decrease with increasing x; for instance, $\Delta a_c = -1.99\%$ and $\Delta V = -5.88\%$ for $x = 0$, $\Delta a_c = -1.36\%$ and $\Delta V = -4.01\%$ for $x = 0.5$, and $\Delta a_c = -0.63\%$ and $\Delta V = -1.87\%$ for $x = 1$. Here, the Δa_c and ΔV values for $Li[Ni_{1/2}Mn_{3/2}]O_4$ are calculated to be −1.98 and −5.83%, respectively, using the reported a_c values before (=8.167 Å) and after (=8.005 Å) the fully charged reaction.[4] Therefore, the Δa_c and ΔV values for $x = 0.5$ are smaller than those for $Li[Ni_{1/2}Mn_{3/2}]O_4$, although the W value for $x = 0.5$ is greater than that for $Li[Ni_{1/2}Mn_{3/2}]O_4$.

It should be noted that the Δa_c and ΔV values for $x = 1$ are significantly smaller compared with those for other positive electrode materials, such as $LiCoO_2$ ($\Delta V \approx +2.5\%$ at the half-charged state)[25] and $LiFePO_4$ ($\Delta V \approx -6.9\%$).[26] The ΔV value of −1.87% for $x = 1$ can be regarded as a "zero-strain" lithium insertion material because one of the zero-strain lithium insertion materials, $Li[CrTi]O_4$, indicates a ΔV of +0.7%.[27,28] Thus far, this statement has not been explicitly expressed, although Alcántara et al.[10] reported the change in a_c for Li_yCoMnO_4.

Zero-strain lithium insertion materials such as $Li[CrTi]O_4$ and $Li[Li_{1/3}Ti_{5/3}]O_4$ (LTO)[29−31] are used as negative electrode materials, whereas the $x = 1$ sample is used as a positive electrode material. XRD and Raman spectroscopy clarified that the zero-strain reaction scheme of LTO is achieved by a change in u on proceeding with the discharge reaction, that is, local structural changes in the LiO_6 and TiO_6 environments.[30,31] To compare with such a zero-strain reaction scheme, u values during various charge states were determined by the Rietveld analyses for $x = 1$. As shown in Figure 8a, u for Li_yCoMnO_4 maintains a constant value (~0.263) up to the fully charged state, suggesting that the zero-strain reaction scheme for $x = 1$ is different from that for LTO. Considering the a_c value (~8.00 Å) at the fully charged state, one can understand the zero-strain reaction scheme for $x = 1$. That is, the minimum a_c value for face-centered cubic (FCC) consisting of only O^{2-} ions is calculated to be ~7.8 Å, using the relations $a_c = 4\sqrt{2}\,r_{O^{2-}}$ and $r_{O^{2-}} = 1.38$ Å (CN = 4) [see Figure 8b]. Hence, the zero-strain character for $x = 1$ is achieved by a rigid framework structure of O^{2-} with FCC packing. In other words, negative electrode materials with zero-strain are due to reversible changes in the local structures, whereas positive electrode materials with zero-strain are due to invariance in the local structures.

Finally, we wish to describe the strategy for positive electrode materials with more high-energy density. Although the $x = 0.5$ sample indicates the maximum W value among the various spinel oxides, its W value is still lower than layered oxides; for instance, layered oxides comprising Li/Ni/Mn/O[2,32] exhibit more than 300 mA h·g^{-1} of Q_{dis} and ~3.5 V of E_{ave}, resulting in more than 1000 mW h·g^{-1} of W. The present findings confirm that the redox reaction of $Co^{3+} \leftrightarrow Co^{4+}$ is effective to increase

DOI: 10.1021/acsomega.7b00948
ACS Omega 2017, 2, 5142−5149

Table 2. Structural Parameters for the Fully Charged $Li_yCo_xMn_{2-x}O_4$ Samples with x = 0, 0.25, 0.5, 0.75, and 1 Determined by the Rietveld Analyses

				atomic coordination			
x in $Li_yCo_xMn_{2-x}O_4$	atom	Wyckoff position	occupancy	x	y	z	B_{iso} (Å^2)
		SG: $Fd\bar{3}m$, a_c = 8.0585(1) Å, R_{wp} = 5.46%, and S = 0.489					
x = 0	Li	8a	0.15	0.125	0.125	0.125	0.86(1)
	Mn	16d	1.00	0.5	0.5	0.5	0.61(1)
	O	32e	1.00	0.262(1)	0.262(1)	0.262(1)	0.87(1)
		SG: $Fd\bar{3}m$, a_c = 8.0525(1) Å, R_{wp} = 5.90%, and S = 0.539					
x = 0.25	Co	16d	0.125	0.5	0.5	0.5	0.45(1)
	Mn	16d	0.875	0.5	0.5	0.5	0.45(1)
	O	32e	1.00	0.263(1)	0.263(1)	0.263(1)	0.52(1)
		SG: $Fd\bar{3}m$, a_c = 8.0196(1) Å, R_{wp} = 7.70%, and S = 0.692					
x = 0.5	Co	16d	0.25	0.5	0.5	0.5	0.37(1)
	Mn	16d	0.75	0.5	0.5	0.5	0.37(1)
	O	32e	1.00	0.263(1)	0.263(1)	0.263(1)	0.50(1)
		SG: $Fd\bar{3}m$, a_c = 8.0109(1) Å, R_{wp} = 11.49%, and S = 1.04					
x = 0.75	Li	8a	0.008	0.125	0.125	0.125	0.76(1)
	Co1	8a	0.030	0.125	0.125	0.125	0.76(1)
	Co2	16d	0.371	0.5	0.5	0.5	0.26(1)
	Mn	16d	0.629	0.5	0.5	0.5	0.26(1)
	O	32e	1.00	0.263(1)	0.263(1)	0.263(1)	0.37(1)
		SG: $Fd\bar{3}m$, a_c = 8.0081(1) Å, R_{wp} = 6.02%, and S = 0.535					
x = 1	Li	8a	0.228	0.125	0.125	0.125	0.43(1)
	Co1	8a	0.113	0.125	0.125	0.125	0.43(1)
	Co2	16d	0.5	0.5	0.5	0.5	0.22(1)
	Mn	16d	0.5	0.5	0.5	0.5	0.22(1)
	O	32e	1.00	0.263(1)	0.263(1)	0.263(1)	0.52(1)

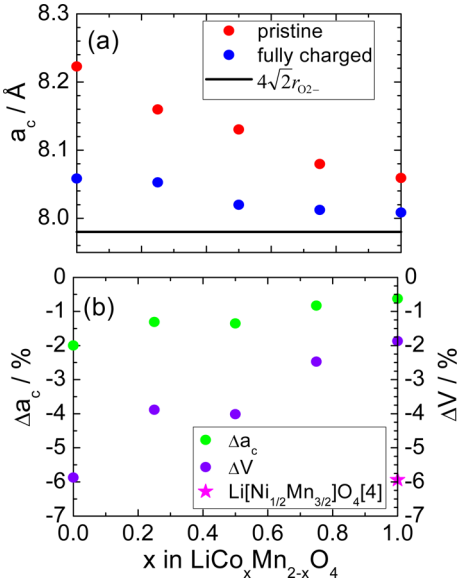

Figure 7. (a) Cubic lattice parameters (a_cs) for the pristine $LiCo_xMn_{2-x}O_4$ samples and fully charged $Li_yCo_xMn_{2-x}O_4$ samples. The solid line in (a) indicates the calculated a_c value from $4\sqrt{2}r_{O^{2-}}$. (b) Change in Δa_c and change in the lattice volume (ΔV) during charge and discharge reactions as a function of x in $LiCo_xMn_{2-x}O_4$. The ΔV value for $Li[Ni_{1/2}Mn_{3/2}]O_4$ was calculated from the data in ref 4.

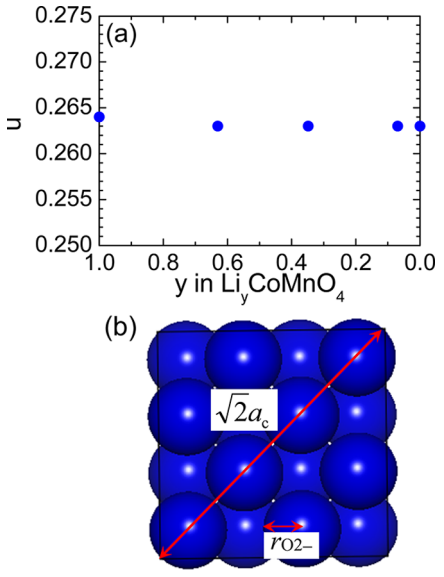

Figure 8. (a) Change in the oxygen positional parameter (u) as a function of y in Li_yCoMnO_4. (b) Schematics of zero-strain reaction scheme for Li_yCoMnO_4. The a_c value (≈8.0 Å) for Li_yCoMnO_4 is close to the minimum lattice parameter ($4\sqrt{2}r_{O^{2-}} \approx 7.8$ Å) for the FCC consisting of O^{2-} ions.

E_{ave}. Thus, layered oxides comprising Li/Co/Mn/O would exhibit greater W values, although the combination of Co and Mn ions in the layered structure is reported to be thermodynamically unstable.[33] Trials for preparing layered Li/Co/Mn/O oxides are underway in our laboratory.

3. CONCLUSIONS

To pair harmoniously with the high W value negative electrode materials, explorations for positive electrode materials with high W values have been performed in a series of LCMO spinels with $0 \leq x \leq 1$. The maximum Q_{dis} value for LCMO was exhibited at x = 0.5, whereas E_{ave} increased monotonically with

DOI: 10.1021/acsomega.7b00948
ACS Omega 2017, 2, 5142−5149

x. Therefore, the maximum W value (=627 mW h·g^{-1}) was obtained at the x = 0.5 composition. The W value for x = 0.5 was slightly greater than that for Li[$Ni_{1/2}Mn_{3/2}$]O_4, which has attracted much attention as a positive electrode material because of its high W value. XRD measurements using synchrotron radiation clarified another advantage for the x = 0.5 sample; that is, the ΔV value for x = 0.5 was about 2% smaller than that for Li[$Ni_{1/2}Mn_{3/2}$]O_4. Thus, the x = 0.5 sample is regarded as a next-generation positive electrode material with a high W value and a long cycle-life. Concerning the ΔV values, the x = 1 sample showed the minimum ΔV value (=−2%) among the various positive electrode materials and can be thought of as a zero-strain lithium insertion material, similar to LTO and Li[CrTi]O_4. The zero-strain character for x = 1 is due to the invariance in the local structures, which is different from those for LTO and Li[CrTi]O_4.

4. EXPERIMENTAL SECTION

4.1. Synthesis and Characterization. Powder samples of LCMO with x = 0, 0.25, 0.375, 0.5, 0.75, and 1 were prepared using a two-step solid-state reaction technique, as reported previously,[4,5,19] to obtain highly crystallized LCMO samples. Regent grade LiOH·H_2O (Wako Pure Chemical Industries, Ltd.), Co_3O_4 (Kojundo Chemical Laboratory Co., Ltd.), and MnO_2 (Kojundo Chemical Laboratory Co., Ltd.) were mixed with a pestle and mortar and then pressed into a pellet of diameter 23 mm and thickness ∼5 mm. The pellet was first sintered at 900 °C for 12 h under flowing oxygen and then heated at 700 °C for 24 h, 600 °C for 24 h, and 500 °C for 48 h, successively, without cooling to room temperature between each temperature step. The heating and cooling rates were 200 and 60 °C·h^{-1}, respectively. The effects of heating temperature were investigated only for x = 1; we set the first sintering temperature to 1000 °C or 1100 °C. A powder sample of Li_2MnO_3 was also synthesized. The reaction mixture of LiOH·H_2O and MnO_2 was heated at 900 °C for 12 h under flowing oxygen.

The obtained LCMO samples with $0 \leq x \leq 1$ were characterized by powder XRD measurements equipped with Fe Kα radiation (D8 ADVANCE, Bruker AXS, Inc.), SEM (S-3600N, Hitachi High-Technologies Co., Ltd.), and Raman spectroscopy (NRS-3300, Jasco Co. Ltd.). XRD measurements were conducted in the 2θ range between 15 and 140° at a step-scan rate of 0.014°. Raman spectroscopy was performed using an excitation wavelength of 532 nm, supplied by a diode-pumped solid-state laser. Before the measurements, the sharp Raman shift of crystalline silicon was calibrated as 520 cm^{-1}. The laser power and duration for taking one Raman spectrum were 1 mW and 720 s, respectively. For the x = 1 sample, a two-dimensional mapping for the Raman spectra was recorded using the excitation wavelength of 532 nm, to obtain information about distributions of $Li_{1-\delta}Co_\delta$[CoMn]O_4 and Li_2MnO_3 phases (inVia Raman microscope, Renishaw plc.). Here, δ is the amount of Co ions at the tetrahedral 8a (Li) site. The area for the Raman mapping was 100 × 25 μm. The laser power and duration for taking one spot of the Raman spectrum were 0.5 mW and 20 s, respectively.

4.2. Electrochemical Measurements. Electrochemical properties for the LCMO samples were examined in a nonaqueous lithium cell. The mixed electrode consisted of 88 wt % LCMO, 6 wt % conducting carbon, and 6 wt % polyvinylidene binder, as reported previously.[5,19] The surface area of the electrode was ∼2.00 cm^2 (ϕ 16 mm). A stainless steel plate (ϕ 19 mm) was pressed onto the lithium metal and used as the counter electrode. The electrolyte was 1 M $LiPF_6$ dissolved in ethylene carbonate (EC)/dimethyl carbonate (DMC) (EC/DMC = 3/7 by volume) solution (KISHIDA Chemical Co. Ltd.). After fabricating the lithium cells in an argon-filled glovebox, the cells were operated at a current of 0.6 mA (≈0.3 mA·cm^{-2}) in the voltage range between 3.0 and 5.4 V. This applied current corresponds to ∼2 C rate. The temperature for the electrochemical measurements was 25 °C.

4.3. Synchrotron Radiation Study. To clarify changes in the crystal structures in the charged states, XRD measurements were also performed at the synchrotron radiation facility, Aichi Synchrotron Radiation Center. All of the charged LCMO samples were prepared using electrochemical reactions and packed into borosilicate capillary tubes with a diameter of 0.3 mm (W. Müller Glas Technik) in the argon-filled glovebox. The XRD patterns were recorded in the 2θ range between 5 and 95° using the two-dimensional detector (PILATUS 100 K, DECTRIS Ltd.) of the BL5S2 beamline. The wavelength of X-ray was determined to be 0.779547(3) Å from the XRD measurement of a silicon standard (NIST 640d). Rietveld analyses were carried out using the RIETAN-FP software,[34] and the schematics of the crystal structures were drawn by the VESTA software.[35] The weight fraction, that is, the mol fraction of the LCMO and Li_2MnO_3 phases were determined by the multiphase mode in the RIETAN-FP program.

■ ASSOCIATED CONTENT

Supporting Information

The Supporting Information is available free of charge on the ACS Publications website at DOI: 10.1021/acsomega.7b00948.

SEM images for the LCMO samples with x = 0.25 and 0.75, charge and discharge curves for the x = 1 samples prepared at the maximum temperatures at 1000 and 1100 °C, results of the Rietveld analyses for the pristine LCMO samples with x = 0.25 and 0.75, weight fraction of the Li_2MnO_3 phase in the LCMO samples, Raman spectra for the LCMO samples with x = 0, 0.25, 0.5, 0.75, and 1, and results of the Rietveld analyses for the fully charged LCMO samples with x = 0.25 and 0.75 (PDF)

■ AUTHOR INFORMATION

Corresponding Author

*E-mail: e1089@mosk.tytlabs.co.jp. Phone: +81-561-71-7698. Fax: +81-561-63-6119 (K.M.).

ORCID

Kazuhiko Mukai: 0000-0002-6154-6539

Notes

The authors declare no competing financial interest.

■ ACKNOWLEDGMENTS

The authors appreciate Dr. Y. Kato and Dr. T. Inoue of TCRDL for help with Raman spectroscopy. The XRD measurements at the Aichi Synchrotron Radiation Center were performed with the approval of the Aichi Science & Technology Foundation, Aichi, Japan, under proposal no. 201605025.

■ REFERENCES

(1) Tarascon, J.-M.; Armand, M. Issues and Challenges Facing Rechargeable Lithium Batteries. *Nature* **2001**, *414*, 359−367.

DOI: 10.1021/acsomega.7b00948
ACS Omega 2017, 2, 5142−5149

(2) Ohzuku, T.; Brodd, R. J. An Overview of Positive-Electrode Materials for Advanced Lithium-Ion Batteries. *J. Power Sources* **2007**, *174*, 449−456.
(3) Zhong, Q.; Bonakdarpour, A.; Zhang, M.; Gao, Y.; Dahn, J. R. Synthesis and Electrochemistry of $LiNi_xMn_{2-x}O_4$. *J. Electrochem. Soc.* **1997**, *144*, 205−213.
(4) Ariyoshi, K.; Iwakoshi, Y.; Nakayama, N.; Ohzuku, T. Topotactic Two-Phase Reactions of $Li[Ni_{1/2}Mn_{3/2}]O_4$ ($P4_332$) in Nonaqueous Lithium Cells. *J. Electrochem. Soc.* **2004**, *151*, A296−A303.
(5) Mukai, K.; Sugiyama, J. An Indicator to Identify the $Li[Ni_{1/2}Mn_{3/2}]O_4$ ($P4_332$): DC-Susceptibility Measurements. *J. Electrochem. Soc.* **2010**, *157*, A672−A676.
(6) Hu, M.; Pang, X.; Zhou, Z. Recent progress in high-voltage lithium ion batteries. *J. Power Sources* **2013**, *237*, 229−242.
(7) Kawai, H.; Nagata, M.; Tukamoto, H.; West, A. R. A New Lithium Cathode $LiCoMnO_4$: Toward Practical 5 V Lithium Batteries. *Electrochem. Solid-State Lett.* **1998**, *1*, 212−214.
(8) Kawai, H.; Nagata, M.; Kageyama, H.; Tukamoto, H.; West, A. R. 5 V Lithium Cathodes Based on Spinel Solid Solutions $Li_2Co_{1+X}Mn_{3-X}O_8$: $-1 \leq X \leq 1$. *Electrochim. Acta* **1999**, *45*, 315−327.
(9) Mandal, S.; Rojas, R. M.; Amarilla, J. M.; Calle, P.; Kosova, N. V.; Anufrienko, V. F.; Rojo, J. M. High Temperature Co-Doped $LiMn_2O_4$-Based Spinels. Structural, Electrical, and Electrochemical Characterization. *Chem. Mater.* **2002**, *14*, 1598−1605.
(10) Alcántara, R.; Jaraba, M.; Lavela, P.; Tirado, J. L. Electrochemical, ^{6}Li MAS NMR, and X-ray and Neutron Diffraction Study of $LiCo_xFe_yMn_{2-(x+y)}O_4$ Spinel Oxides for High-Voltage Cathode Materials. *Chem. Mater.* **2003**, *15*, 1210−1216.
(11) Hu, M.; Tian, Y.; Su, L.; Wei, J.; Zhou, Z. Preparation and Ni-Doping Effect of Nanosized Truncated Octahedral $LiCoMnO_4$ As Cathode Materials for 5 V Li-Ion Batteries. *ACS Appl. Mater. Interfaces* **2013**, *5*, 12185−12189.
(12) Julien, C. M.; Mauger, A. Review of 5-V Electrodes for Li-Ion Batteries: Status and Trends. *Ionics* **2013**, *19*, 951−988.
(13) Hu, M.; Tian, Y.; Wei, J.; Wang, D.; Zhou, Z. Porous Hollow $LiCoMnO_4$ Microspheres As Cathode Materials for 5 V Lithium Ion Batteries. *J. Power Sources* **2014**, *247*, 794−798.
(14) Zhecheva, E.; Stoyanova, R.; Alcántara, R.; Lavela, P.; Tirado, J. L. EPR Studies of Li Deintercalation from $LiCoMnO_4$ Spinel-Type Electrode Active Material. *J. Power Sources* **2006**, *159*, 1389−1394.
(15) Stoyanova, R. K.; Zhecheva, E. N.; Gorova, M. Y. EPR Evidence on Short-Range Co/Mn Order in $LiCoMnO_4$ Spinels. *J. Mater. Chem.* **2000**, *10*, 1377−1381.
(16) Amdouni, N.; Gendron, F.; Mauger, A.; Zarrouk, H.; Julien, C. M. $LiMn_{2-y}Co_yO_4$ ($0 \leq y \leq 1$) Intercalation Compounds Synthesized from Wet-Chemical Route. *Mater. Sci. Eng., B* **2006**, *129*, 64−75.
(17) Ariyoshi, K.; Maeda, Y.; Kawai, T.; Ohzuku, T. Effect of Primary Particle Size upon Polarization and Cycling Stability of 5-V Lithium Insertion Material of $Li[Ni_{1/2}Mn_{3/2}]O_4$. *J. Electrochem. Soc.* **2011**, *158*, A281−A284.
(18) Smereka, P.; Li, X.; Russo, G.; Srolovitz, D. J. Simulation of Faceted Film Growth in Three Dimensions: Microstructure, Morphology and Texture. *Acta Mater.* **2005**, *53*, 1191−1204.
(19) Mukai, K.; Sugiyama, J.; Ikedo, Y.; Nozaki, H.; Kamazawa, K.; Andreica, D.; Amato, A.; Månsson, M.; Brewer, J. H.; Ansaldo, E. J.; Chow, K. H. Microscopic Magnetic Study on the Nominal Composition $Li[Li_{1/3}Mn_{5/3}]O_4$ by Muon-Spin Rotation/Relaxation Measurements. *J. Phys. Chem. C* **2010**, *114*, 11320−11327.
(20) Iwata, E.; Takeda, S.; Iwanaga, M.; Ohzuku, T. XRD Observation on Fully-Charged $Li[Li_yMn_{2-y}]O_4$ in Nonaqueous Lithium Cells. *Electrochemistry* **2003**, *71*, 1187−1191.
(21) Mukai, K.; Sugiyama, J.; Kamazawa, K.; Ikedo, Y.; Andreica, A.; Amato, A. Magnetic Properties of the Chemically Delithiated $Li_xMn_2O_4$ with $0.07 \leq x \leq 1$. *J. Solid State Chem.* **2011**, *184*, 1096−1104.
(22) Bhagavantam, S.; Venkatarayudu, T. *Theory of Groups and Its Application to Physical Problems*; Academic Press: New York, 1969; pp 140−158.
(23) Julien, C. M.; Massot, M. Lattice Vibrations of Materials for Lithium Rechargeable Batteries I. Lithium Manganese Oxide Spinel. *Mater. Sci. Eng., B* **2003**, *97*, 217−230.
(24) Shannon, R. D. Revised Effective Ionic Radii and Systematic Studies of Interatomic Distances in Halides and Chalcogenides. *Acta Crystallogr., Sect. A: Cryst. Phys., Diffr., Theor. Gen. Crystallogr.* **1976**, *32*, 751−767.
(25) Ohzuku, T.; Ueda, A. Solid-State Redox Reactions of $LiCoO_2$ ($R\bar{3}m$) for 4 Volt Secondary Lithium Cells. *J. Electrochem. Soc.* **1994**, *141*, 2972−2977.
(26) Padhi, A. K.; Nanjundaswamy, K. S.; Goodenough, J. B. Phospho-Olivines as Positive-Electrode Materials for Rechargeable Lithium Batteries. *J. Electrochem. Soc.* **1997**, *144*, 1188−1194.
(27) Ohzuku, T.; Tatumi, K.; Matoba, N.; Sawai, K. Electrochemistry and Structural Chemistry of Li[CrTi]O4 ($Fd\bar{3}m$) in Nonaqueous Lithium Cells. *J. Electrochem. Soc.* **2000**, *147*, 3592−3597.
(28) Mukai, K.; Ariyoshi, K.; Ohzuku, T. Comparative Study of $Li[CrTi]O_4$, $Li[Li_{1/3}Ti_{5/3}]O_4$ and $Li_{1/2}Fe_{1/2}[Li_{1/2}Fe_{1/2}Ti]O_4$ in Non-Aqueous Lithium Cells. *J. Power Sources* **2005**, *146*, 213−216.
(29) Ohzuku, T.; Ueda, A.; Yamamoto, N. Zero-Strain Insertion Material of $Li[Li_{1/3}Ti_{5/3}]O_4$ for Rechargeable Lithium Cells. *J. Electrochem. Soc.* **1995**, *142*, 1431−1435.
(30) Ariyoshi, K.; Yamato, R.; Ohzuku, T. Zero-Strain Insertion Mechanism of $Li[Li_{1/3}Ti_{5/3}]O_4$ for Advanced Lithium-Ion (Shuttlecock) Batteries. *Electrochim. Acta* **2005**, *51*, 1125−1129.
(31) Mukai, K.; Kato, Y.; Nakano, H. Understanding the Zero-Strain Lithium Insertion Scheme of $Li[Li_{1/3}Ti_{5/3}]O_4$: Structural Changes at Atomic Scale Clarified by Raman Spectroscopy. *J. Phys. Chem. C* **2014**, *118*, 2992−2999.
(32) Ohzuku, T.; Nagayama, H.; Tsuji, K.; Ariyoshi, K. High-Capacity Lithium Insertion Materials of Lithium Nickel Manganese Oxides for Advanced Lithium-Ion Batteries: Toward Rechargeable Capacity More Than 300 mA h g^{-1}. *J. Mater. Chem.* **2011**, *21*, 10179−10188.
(33) Li, W.; Song, B.; Manthiram, A. High-Voltage Positive Electrode Materials for Lithium-Ion Batteries. *Chem. Soc. Rev.* **2017**, *46*, 3006−3059.
(34) Izumi, F.; Momma, K. Three-Dimensional Visualization in Powder Diffraction. *Solid State Phenom.* **2007**, *130*, 15−20.
(35) Momma, K.; Izumi, F. VESTA 3 for Three-Dimensional Visualization of Crystal, Volumetric and Morphology Data. *J. Appl. Crystallogr.* **2011**, *44*, 1272−1276.

DOI: 10.1021/acsomega.7b00948
ACS Omega 2017, 2, 5142−5149